

Impurity States in Graphene

T.O. Wehling,¹ A.V. Balatsky,² M.I. Katsnelson,³ A.I. Lichtenstein,¹ K. Schamberg,¹ and R.W. Jesendanger⁴

¹I. Institut für Theoretische Physik, Universität Hamburg, Jungiusstraße 9, D-20355 Hamburg, Germany

²Theoretical Division, Los Alamos National Laboratory, Los Alamos, New Mexico 87545, USA

³Institute for Molecules and Materials, University of Nijmegen,
Toernooiveld 1, 6525 ED Nijmegen, The Netherlands

⁴I. Institut für Angewandte Physik, Universität Hamburg, Jungiusstraße 11, D-20355 Hamburg, Germany

(dated: 23rd March 2024)

Defects in graphene are of crucial importance for its electronic and magnetic properties. Here impurity effects on the electronic structure of surrounding carbon atoms are considered and the distribution of the local densities of states (LDOS) is calculated. As the full range from near field to the asymptotic regime is covered, our results are directly accessible by scanning tunnelling microscopy (STM). We also include exchange scattering at magnetic impurities and elucidate how strongly spin polarized impurity states arise.

Graphene, a recently discovered allotrope of carbon and the first known example of a truly two-dimensional (2D) crystal [1, 2] has unique electronic properties [3, 15], such as an exotic quantum Hall effect with half-integer quantization of the Hall conductivity [3, 4], finite conductivity at zero charge-carrier concentration [3], strong suppression of weak localization [12], etc. The peculiar 2D band structure of graphene resembles ultrarelativistic electron dynamics near two nodal points in the Brillouin zone. This provides a new bridge between condensed matter theory and quantum electrodynamics (index theorem and the half-integer quantum Hall effect [3], relativistic Zitterbewegung [16] and the minimal conductivity [11], "Klein paradox" [17] and anomalous tunnelling of electrons in graphene through potential barriers [15]). Unexpectedly high electron mobility in graphene and its perfect suitability for planar technology makes it a perspective material for a next-generation, carbon-based electronics [1].

Impurity states are important contributors to these unusual properties. Graphene is conducting due to carriers that can either be introduced by a gate voltage [1, 3, 4] or by doping [1, 8, 9]. This situation is very reminiscent of doped semiconductors, where the desired properties are obtained by creating an impurity band. Recent progress in scanning tunneling microscopy (STM) made it possible to image impurity states for a wide class of materials with very high spatial resolution. This so-called "wave function imaging" yields local images of the impurity-induced wave function. Examples of wave function imaging range from unconventional superconductors [18, 19] to semiconductors [20, 21], magnetic metals [22] and graphite surfaces [23–25]. It allows one to investigate the formation of the impurity band and the associated electronic properties. Theoretical modelling and STM measurements of near impurity site effects can be compared and thus elucidate, e.g., magnetic interaction mechanisms [21, 26].

The purpose of this letter is to address the question of electronic properties of single and double impurities in graphene in connection with future STM experiments

and impurity-induced ferromagnetism. The impurity states are characterized by their energy and by their real space wave functions that determine the shape of the resonance. In contrast to previous studies [9, 14] we consider the real space structure of the electronic state in the range from the impurity site to the asymptotic regime, its dependence on the potential strength and the spin exchange interaction. We will address the impurity states as an input into a subsequent discussion of impurity-induced bands.

The honeycomb arrangement of carbon atoms in graphene can be described by a hexagonal lattice with two sublattices A and B. (See, e.g., [27]). With the Fermi operators c_i and d_i of electrons in cell i at sublattice A and B, respectively, we describe a single and two neighbouring impurities by $V_s = U_0 c_0^\dagger c_0$ and $V_d = U_0 (c_0^\dagger c_0 + d_0^\dagger d_0) + U_1 (c_0^\dagger d_0 + d_0^\dagger c_0)$. Here U_0 is the potential strength and U_1 the change of sublattice hopping between the two impurity sites. Related to the current research are questions about impurities in graphite that have been studied with STM [23]. Only the atoms above hollow sites are seen in STM on graphite. We find that impurity states in graphene are qualitatively different from those in graphite because of the sublattice degeneracy that is reflected in a complicated sublattice structure of impurity-induced resonances.

We find that impurity scattering produces low energy resonances with the real space structure and the resonant energy E_{imp} as function of U_0 (and U_1) clearly distinguishing between single and double impurities. For single impurities we find in agreement with Loktev [10], that E_{imp} is well described by

$$U_0 = \frac{W^2}{E_{\text{imp}} \ln \frac{E_{\text{imp}}^2}{W^2 - E_{\text{imp}}^2}}; \quad (1)$$

where W is the band width. Hence the resonance energy E_{imp} approaches zero for $U_0 \rightarrow 1$. Only strong single impurities (i.e. $U_0 > 10 \text{ eV}$) are capable of producing resonances within 1 eV of the Dirac point. This result is

similar to the impurity states observed in unconventional superconductors with Dirac spectrum [28].

The resonance of a double impurity is basically determined by $U_0 - U_1$. Its energy coincides with the Dirac point at finite $U_0 - U_1 = 3t$, where $t = 2.7$ eV is the nearest neighbour hopping parameter of graphene.

We give a detailed description of the local density of states (LDOS), the real space fingerprint of impurities in graphene, both near the impurity and in the asymptotic regime at large distances. Near the impurity site that LDOS exhibits an intricate pattern. A single strong impurity placed on one sublattice produces a peak in LDOS at low energies that is large on the other sublattice. At large distances these impurity resonances have wave functions that asymptotically decay as $j^2 / 1=r$.

We will consider potential scattering (nonmagnetic) as well as a magnetic impurities, i.e. spin dependent scattering. In the latter case the impurity induced resonance will exhibit a spin dependent splitting that might lead to a strong spin polarization of the impurity state. This observation, we believe, is important for the discussion of magnetism and possible magnetic order in graphene.

To start with our theoretical model, we describe the carbon p_z -electrons within the tight binding approximation by $H = \sum_{\mathbf{k}} \frac{d^2 \mathbf{k}}{B} \psi(\mathbf{k}) H_{\mathbf{k}} \psi(\mathbf{k})$ with $\psi(\mathbf{k}) = \begin{pmatrix} c(\mathbf{k}) \\ d(\mathbf{k}) \end{pmatrix}$ and $H_{\mathbf{k}} = \begin{pmatrix} 0 & t(\mathbf{k}) \\ t(\mathbf{k}) & 0 \end{pmatrix}$, where $t(\mathbf{k}) = \frac{P}{3} \sum_{j=1}^3 e^{ik_j(b_j - b_1)}$. B denotes the Brillouin zone volume and $c(\mathbf{k})$ ($d(\mathbf{k})$) are the k -space counterparts of c_i (d_i). [27]

The full Green's function in real space $G(i; j; E)$ will be obtained using the T-matrix formalism:

$$G(i; j; E) = G^0(i; j; E) + G^0(i; E) T(E) G^0(j; E). \quad (2)$$

Therefore the unperturbed Green's function $G^0(i; E)$ in real space is calculated from its k -space counterpart $G^0(\mathbf{k}; E) = (E - H_{\mathbf{k}} + i\epsilon)^{-1}$ by Fourier transformation. Numerical problems in carrying out the Fourier integrals are avoided, by linearizing the bandstructure in a vicinity of the Dirac points, where all singularities occur. Outside these regions the full tight-binding bandstructure is taken into account. Finally the T-matrix is given by

$$T(E) = \frac{1}{V_{s(d)} G^0(0; E)} \frac{1}{V_{s(d)}} \quad (3)$$

with $V_s = U_0 \begin{pmatrix} 1 & 0 \\ 0 & 0 \end{pmatrix}$ and $V_d = \begin{pmatrix} U_0 & U_1 \\ U_1 & U_0 \end{pmatrix}$ being the impurity potentials in k -space and matrix form. Poles of the T-matrix corresponding to impurity resonances occur, if $\det(1 - V_{s(d)} G^0(0; E)) = 0$, i.e.

$$U_0 G_{11}^0(0; E) - 1 = 0 \quad (4)$$

for a single scatterer and

$$(1 - U_0 G_{11}^0(0; E))^2 - U_0^2 G_{21}^0(0; E) G_{12}^0(0; E) = 0 \quad (5)$$

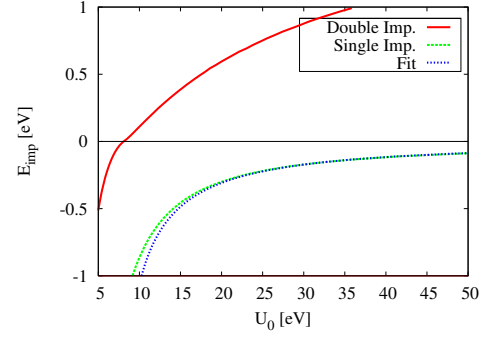


Figure 1: (Color online) The energy E_{imp} of the impurity resonance as function of the potential strength U_0 is shown for single impurities and double impurities with $U_1 = 0$. For the single scatterer E_{imp} obtained from our tight binding calculation is compared to the result obtained from the fully linearized bandstructure (Eqn. 1) with fitted bandwidth $W = 6.06$ eV.

for double impurity with $U_1 = 0$ | this case, we refer to as scalar impurity. Near the Dirac points we have $\text{Re}(G^0) \propto \text{Im}(G^0)$ so that the impurity resonances E_{imp} as function of U_0 can be calculated from the previous two equations considering only the $\text{Re}(G^0)$: The resulting real impurity energies as a function of U_0 are shown in Figure 1. Adjusting the bandwidth parameter W in Eqn. (1) to fit our $E_{\text{imp}}(U_0)$ yields $W = 6.06 \pm 0.02 \text{ eV}$. W differs slightly from the bandwidth $\bar{W} = \hbar v_F \frac{\pi}{2a} = 6.3 \text{ eV}$ obtained by assuming linear dispersion in the entire Brillouin zone. [10]

It is quite remarkable that a pair of neighbouring scatterers produces a resonance at the Dirac point for $U_0 = 3t = 8.1 \text{ eV}$, while for a single impurity this occurs only in the limit of infinite potential strength. This effect can be attributed to the existence of two nonequivalent Dirac points in the Brillouin zone. As a consequence at $E = 0$ the onsite Green's function $G^0(0; 0)$ has finite diagonal $G_{12}^0(0; 0) = G_{21}^0(0; 0) = \frac{1}{3t}$ but vanishing diagonal components resulting via equations 4 and 5 in the characteristic $E_{\text{imp}}(U_0)$ curves.

For double impurities with sublattice hopping change U_1 , it follows directly from the secular equation, that the impurity energy as a function of U_0 and U_1 is obtained from the scalar case by replacing U_0 with $U_0 - U_1$.

We obtained the LDOS $N(\mathbf{r}; E) = \frac{1}{\text{Im}} \sum_{i,j} \psi_i(\mathbf{r}) G(i; j; E) \psi_j^*(\mathbf{r})$ in presence of impurities as a function of position and energy, where $\psi_i(\mathbf{r}) = \begin{pmatrix} c_i(\mathbf{r}) \\ d_i(\mathbf{r}) \end{pmatrix}$ with $c_i^{\text{cd}}(\mathbf{r})$ being carbon p_z -orbitals located in the unit cell i at sublattice A and B respectively. This LDOS of impurity resonances at $E_{\text{imp}} = 0.1 \text{ eV}$ for a single and scalar impurities are shown in Figure 2. [29] The formation of virtual bound states (VBS) due to impurity scattering is clearly visible.

These VBS are a general feature of localized states hybridizing with a continuum of delocalized states. They

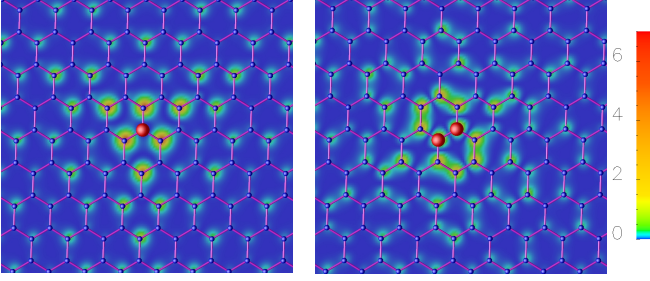


Figure 2: (Color online) r -dependent LDOS at $E = E_{\text{imp}} = 0.1 \text{ eV}$ for a single impurity with $U_0 = 45 \text{ eV}$ (left) and for a scalar double impurity with $U_0 = 6.9 \text{ eV}$ (right) encoded corresponding to color bar. The impurity sites are marked as big red dots in the center of the images.

have been observed in many systems ranging from elementary metals [30] to d-wave superconductors [28]. Details of the real space image are however system specific. Here, the threefold (D_{3h}) symmetry of the VBS for a single impurity and twofold (D_{2h}) symmetry for a double impurity are direct consequences of the lattice symmetry. The (D_{3h}) symmetric single impurity state results in sixfold symmetric Fourier transformed scanning tunnelling spectra [31]. Furthermore the peculiarities of the bandstructure of graphene manifest themselves in the near field characteristics of impurities: A single impurity in sublattice A induces an impurity state mostly localized in sublattice B and vice versa due to the fact that $G_{11}^0(i;E) = G_{12}^0(i;E); G_{21}^0(i;E)$ for $E \neq 0$, which can be attributed to the existence of two nonequivalent Dirac points as explained above.

The site projected DOS $N(i;E)$ can be obtained from the full Green's function $N(i;E) = -1/\pi \text{Im} G(i;i;E)$, where each of the diagonal matrix elements corresponds to one sublattice. For the single impurity and U_0 from 10 eV to 40 eV the LDOS at the impurity, nearest neighbour (NN) and next NN sites are shown in Figure 3. One sees that for vacancies with $10 \text{ eV} < U_0 < 20 \text{ eV}$ [8], but not for weaker potentials, an impurity resonance should be clearly observable within 1 eV around the Dirac point.

It further illustrates the localization of the impurity state on sublattice B, when the impurity is in sublattice A, as well as the reduction of LDOS at the impurity site for strong repulsive potential. The double impurity respects pseudospin symmetry and is much more sensitive to weaker potentials as can be seen from Figure 4. Clearly, $U_t = U_0 - U_1$ is the most important parameter determining the shape of LDOS in the case of a double impurity: The results for $(U_0 = 4 \text{ eV}, U_1 = -2 \text{ eV})$ and $(U_0 = 6 \text{ eV}, U_1 = 0 \text{ eV})$ are virtually indistinguishable at the impurity resonance but differ slightly below it. For large distances $r \gg \hbar v_F/E_{\text{imp}}$ from the impurity site we obtain for the changes in LDOS $N(r;E_{\text{imp}})/1=r$ in agreement with [31, 32] for all considered types of impurities. Note the contrast to a single hard-wall impurity,

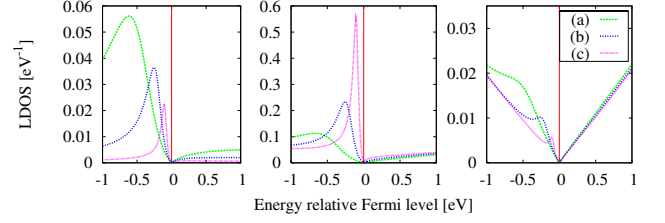


Figure 3: (Color online) LDOS at the impurity site (left), NN (middle) and NNN sites (right) is shown for a single impurity with potential $U_0 = 10 \text{ eV}$ (a), 20 eV (b) and 40 eV (c).

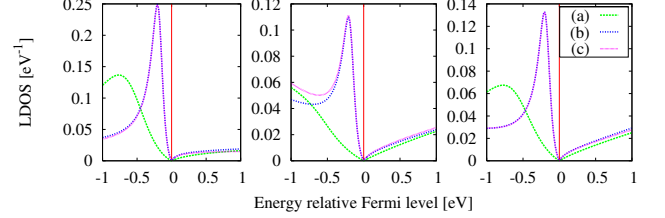


Figure 4: (Color online) As Figure 3 but for scalar double impurity with $U_0 = 4 \text{ eV}$ (a) and 6 eV (c) as well as for double impurity with $U_0 = 4 \text{ eV}$ and $U_1 = -2 \text{ eV}$ (b).

ie. $U_0 \ll 1$, with $1=r^2$ asymptotics of $N(r;E_{\text{imp}})$ [7].

If the impurities have a magnetic moment, exchange scattering of the graphene p_z -electrons and the spin S localized at the impurity site will occur. As long as the exchange coupling J does not exceed a critical value, Kondo screening of the spin S by the band electrons can be neglected and the impurity spin acts as local magnetic field: The effective scattering potential is renormalized to $U_0 - J$. The resulting change in spin-polarized (SP) LDOS in the vicinity of a single impurity is shown in Figure 5 for $U_0 = 12 \text{ eV}$ and $J = 2 \text{ eV}$. The exchange splitting of the resonances in the two spin channels is approximately 0.15 eV. This type of exchange scattering also affects decay lengths and oscillation periods of the induced spin density variations and therefore provides a possible mechanism for long range exchange interactions.

For double impurities the effect of exchange splitting is much more pronounced within a realistic parameter

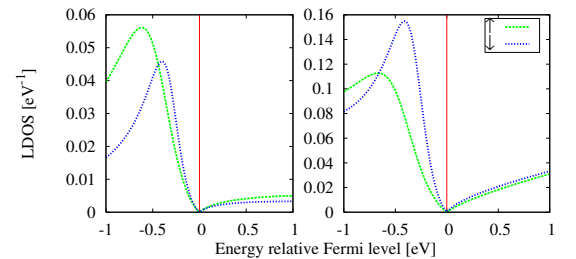


Figure 5: (Color online) SP-LDOS at the impurity site (left) and a NN site (right) is shown for a single magnetic impurity with $U_0 = 12 \text{ eV}$ and $J = 2 \text{ eV}$.

